Effect of Reynolds number on dynamics of a vortex-ring interacting with a flat wall

Heng Ren

Abstract— **The interaction of a vortex ring with a flat wall in three dimensions is investigated using large eddy simulation (LES). We consider the effect of Reynolds number on the dynamics of vortex structures and the turbulent behaviour of flow. For high Reynolds number case, the total kinetic energy decreasing more quickly and larger amplitude of the enstrophy indicates that the flow dissipates more quickly. After the vortical structures break into small-scale vortices, the transition from laminar to turbulent state occurs. The turbulent behaviour can be analysed by the turbulent kinetic energy. Larger amplitude of the TKE indicates the stronger strength of turbulence for the high Reynolds number case. Moreover, it is found that the formation of the loop-like and hair-pin vortices plays an important role in the flow transition from laminar to turbulent state.**

Index Terms— **Vortex ring, flat wall, large eddy simulation, turbulence, vortex structures.**

[1] INTRODUCTION

The interaction of vortical structures with solid boundaries is a fundamental fluid dynamic topic which has received considerable attention in recent years. The interest in this subject is partly due to several practical applications, (e.g. impact of helicopter rotor vortices with following rotor blades or with the vehicle airframe, chopping of a pump intake vortex by the turbine blades, and interaction of an aircraft trailing vortex with a following aircraft or with the airstrip during landing and take-off), and partially in order to gain a better insight in the fundamental dynamics of vorticity in such flow situations. As one of the simplest and important forms of vortex motion, vortex rings widely exist in nature. The interaction of vortex rings with solid boundaries is an important problem in fluid dynamics. This subject is also associated with a variety of practical applications, such as vortex rings extinguishing gas and oil well fires [1], cavitated rings used for underwater drilling [2], and modeling the interaction between the downburst and the aircraft [3]. Moreover, the underlying flow phenomena and physical mechanisms are still unclear and are of great interest for detailed studies.

Vortex rings interacting with a flat wall has been extensively studied. These studies [4-9] showed that as the primary vortex ring moves gradually toward the wall, its rate of approach slows and its radius continues to increase; meanwhile, considerable secondary vorticity is generated on the surface. When the Reynolds number, based on the initial diameter and translational speed of the vortex ring, is larger than about 500, the secondary vorticity separates from the surface and interacts with the primary vortex ring resulting in the ring rebounding from the wall. Actually, these studies are mainly limited to relatively low Reynolds numbers, the highest Reynolds number in these studies is about 2840 [9]. The experimental study [9] has revealed that, beyond Re = 3000 for the interaction between a vortex ring and a flat wall, the primary vortex ring will no longer remain stable as it approaches the wall.

For the instability of a free vortex ring, there are theoretical, experimental, and numerical studies [10-11]. While the azimuthal instability of a vortex ring impinging on a solid wall has been examined, to our knowledge, only in the experimental study by Walker et al. [9] and numerical studies by Olandi et al. [6]. In this letter, we investigate the effect of Reynolds number on the dynamics of vortex structures and turbulent behaviour of flow during the vortex-ring/wall interaction.

[2] NUMERICAL METHOD

To investigate a vortex ring impinging on a curved surface, the three-dimensional Favre-filtered compressible Navier-Stokes equations in generalized coordinates are employed. The equation of state for an ideal gas is used and the molecular viscosity is assumed to obey the Sutherland law. To non-dimensionalize the governing equations, the radius of the initial vortex ring and the far-field variables are used as characteristic quantities. It should be indicated that, similar to LES on the evolution of longitudinal stationary vortices [12], the present simulation is for a low Mach number of 0.3 based on the far-field speed of sound, which is very near the incompressible limit. Sreedhdar and Ragab [12] have verified that the approach based on the compressible N-S equations can reliably predict the incompressible flow characteristics of the vortex evolution.

The large eddy simulation is implemented for turbulence closure. In order to model some terms in the Favre-filtered equations arising from the unresolved scales, dynamic subgrid-scale (SGS) models for turbulent flows are employed. A detailed description of the mathematical formulation of the governing equations and the SGS models have been given in our previous paper [13-14].

The governing equations are numerically solved by a finite-volume method. As employed in our previous work [13-14], the convective terms are discretized by a second-order central scheme and the viscous terms by a fourth-order centered scheme. Time advancement is performed by an implicit approximate factorization method

Manuscript received July, 2017.

***Heng Ren**, China Electronics Technology Group Corporation No.38 Research Institute, Hefei, China, +86 18900518514.*

ISSN: 2278 – 7798

with sub iterations to ensure a second-order accuracy. Moreover, the present numerical methods have already been used successfully to a variety of turbulent flows and have been verified to provide the reliable calculations.

[3] COMPUTATION MODEL AND BOUNDARY CONDITIONS

As illustrated in Fig. 1, a vortex ring of radius R_0 is initially placed at $\boldsymbol{x_c} = (0, 0, H)$, H is the distance between the vortex ring center and the wall.

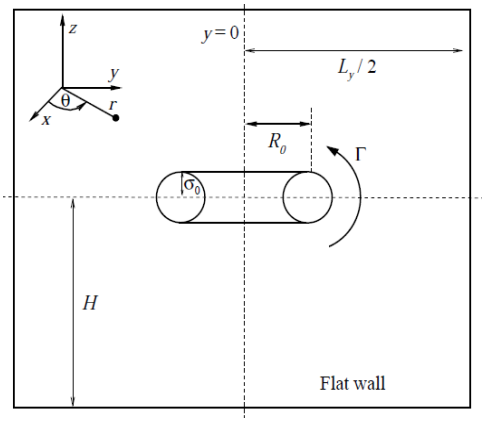

Fig. 1. Schematic diagram of a vortex ring approaching a flat wall.

The initial vorticity distribution of the vortex ring is assigned by a Gaussian function. The initial translational speed of the vortex ring can be represented as

$$u_v = \frac{\Gamma}{4\pi R_0}(\ln\frac{8R_0}{\sigma_0} - \frac{1}{4}), \qquad (1)$$

where σ_0 is the initial core radius and Γ is the circulation of the vortex ring. To deal with the instability of the vortex ring, an azimuthal disturbance with an amplitude of 2×10^{-4} is introduced by imposing a radial displacement on the axis of the ring.

In the computation, we calculate two cases with $Re = 2 \times 10^4$ and $Re = 5 \times 10^4$ respectively. Case 1 represents the low Reynolds number case and case 2 represents the relative high Reynolds number case. For both cases, slenderness ratio of the vortex ring is $\sigma_0 / R_0 = 0.2$, the initial translational speed of the ring is $u_s = 0.3$ and $H = 3R_0$.

The computational domain extends for 16 ring radii in the x and y directions and 12 radii in the vertical direction, with $L_x/R_0 = L_y/R_0 = 16$, $L_z/R_0 = 12$. Based on our careful examinations, a mesh of size $N_x \times N_y \times N_z = 641 \times 641 \times 263$ with resolution $R_0 = 40\Delta x$ is used in the computation, where N_x and N_y are dimensions of the mesh in two horizontal directions x and y, and and N_z is the dimension in the vertical direction z. The grid-spacing is uniform in x and y, and grid stretching is employed in z to increase the grid resolutions near the surface. In the transversal x and y directions, periodicity boundary conditions are used. In the vertical z direction, the flow is bounded by a no-slip wall on the bump surface and far-field boundary condition at $z = L_z$.

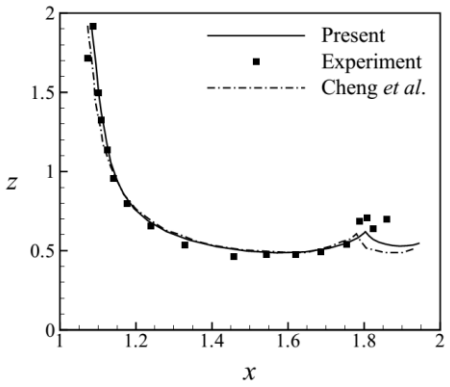

Fig. 2. The trajectory of the primary ring center for $Re = 830$. The solid and dashdot lines present the numerical results obtained in this work and by Cheng *et al.* respectively. The symbol represents the experimental data.

We will validate our code by a comparison with the existing results for a vortex ring impacting a flat wall at $Re = 830$. For the vortex ring/wall interacting case, the initial conditions are the same with experiment by Chu *et al.* [8]. The Gaussian ring is initially placed at the vertical position $h = 3R_0$ and we use the grid resolution $R_0 = 30\Delta x$ for the simulation which is same with the cases in Cheng *et al.* [4]. We compare the trajectory of the primary vortex ring center with the experiment and the numerical study, as shown in Fig. 2. Clearly, our results are convergent to the experimental data and better than numerical results by Cheng *et al.* using Lattice Boltzmann method.

[4] RESULTS AND DISCUSSION

To investigate the global behavior of flow evolution, we further analyze the total kinetic energy and enstrophy in the flow field. Here, the kinetic energy E and enstrophy Ω are defined as

$$E = \frac{1}{2}\int (\mathrm{u}\cdot\mathrm{u})dV, \quad \Omega = \frac{1}{2}\int (\omega\cdot\omega)dV$$

where the integral domain is the whole flow field. The total kinetic energy and enstrophy are shown in figure 3. It is seen from figure 3(a) that the kinetic energy essentially decreases with the flow evolution due to the viscous dissipation. Comparing with the three evolution phases (approach, slowing and collision) of the vortices, the kinetic energy reduces smoothly during the separation of boundary layer and the generation of secondary vortex and decreases quickly as the vortices break down into small-scale ones. Comparing with case 1, it is found that the total kinetic energy decreases more quickly for case 2, indicating that the flow dissipates more quickly for high Reynolds number case.

Figure 3(b) shows the time-dependent enstrophy, which is closely associated with the evolution of vortices. Here we can reasonably clarify three distinct phases of the evolution of the secondary vortex, i.e., generation, deformation and breakdown, corresponding to the three typical evolution phases of the vortices. Before t=18 approximately, the vortex ring is somewhat far from the wall and the enstrophy is almost constant. During $18 < t < 24$, the enstrophy grows considerably due to the separation of boundary layer and the generation of secondary vortex on the surface. Then, because of the secondary vortex ring interacting with wall, the enstrophy decreases. Then with the generation of the tertiary

ISSN: 2278 – 7798

and fourth vortices induced by the primary vortex ring as well as the stretching and deformation of the primary and secondary vortices, the enstrophy continuously increases and reaches its maximum at approximately t=38 for case 1 and t=36 for case 2. Then, as the vortices break down into small-scale ones, the enstrophy decreases quickly. Figure 4 shows the evolution of three-dimensional vortex structures depicted by isosurface of the Q-criterion for the two cases at t=40. It is seen that there are more small-scale vortices for case 1 than case 2, indicating the flow dissipates more quickly for higher Reynolds number case.

After the vortical structures break into small-scale vortices, the transition from laminar to turbulent state occurs. To investigate the flow evolution and the relevant turbulent behaviour, we analyse the turbulent kinetic energy (TKE), which is defined as

$$TKE = \frac{1}{2}\int (\mathrm{u}' \cdot \mathrm{u}')dV$$

Figure 5 shows the evolution of TKE. For the low Reynolds number (case 1), during the approach and early slowing phases, the value of turbulent kinetic energy remains at zero, corresponding to the laminar flow state. It is seen that the generation of secondary vortex ring at t=23 approximately is an indication of the growth of TKE. Then with the development of the azimuthal instability in the vortex structures and the breakdown of these structures, the TKE grows rapidly and reaches its maximum value at approximately t=38, representing the flow transition to turbulence. After t=38, the TKE decays rapidly due to the vortical evolution and the viscous decay. For case 2, the larger amplitude of the TKE indicates the stronger strength of turbulence for the high Reynolds number case.

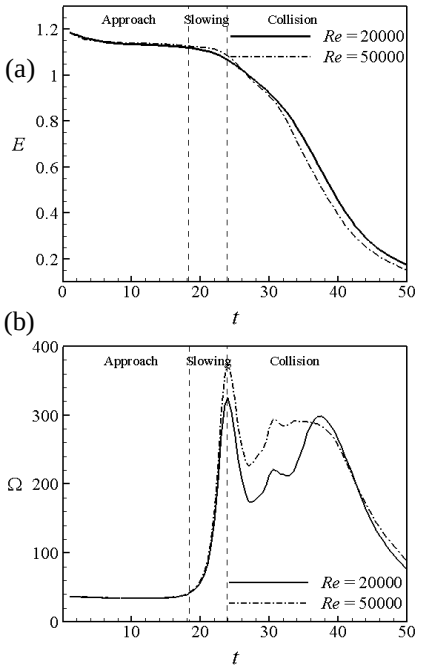

Fig. 3. (a) Kinetic energy E and (b) enstrophy Ω in the flow field. Three phases are described as approach (I), slowling (II), and collision (III).

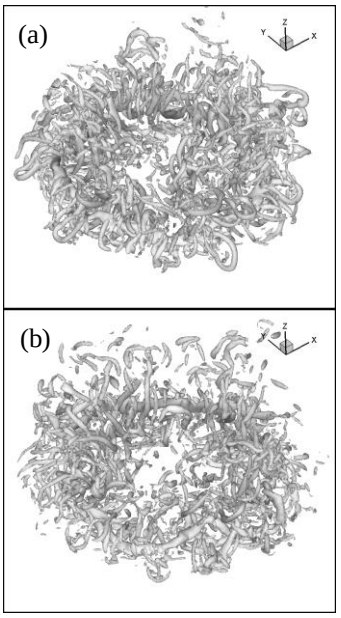

Fig. 4. Vortex structures shown by isosurface of the Q-criterion (Q=4) at t=40. (a) Re=20000, (b) Re=50000.

According to the investigation of an isolated vortex ring transition from the laminar to the turbulent state, the shedding of hair-pin vortices along the azimuthal direction of the ring indicates the turbulent flow state. In present study, two typical vortical structures, i.e., the loop-like vortices and hair-pin vortices, are identified, which play a similar role in the occurrence of turbulent flow state. As both the loop-like and hair-pin vortices are mainly distributed by the vorticity components in the radial and vertical directions, we can reasonably measure the strength of these vortices by integrating the enstrophy in the whole flow field,

$$\Omega_{rz} = \frac{1}{2}\int (\omega_r^2 + \omega_z^2)dV$$

The evolution of Ω_{rz} is shown in figure 5. Compared with the profiles of TKE , it is interesting to notice that the time-dependent characters of both Ω_{rz} and TKE exhibit the similar manner. The generation of Ω_{rz} (or the loop-like vortices and hair-pin vortices) corresponds to the instant of the growth of TKE. This behaviour reasonably indicates that the formation of the loop-like and hair-pin vortices plays an important role in the flow transition from laminar to turbulent state.

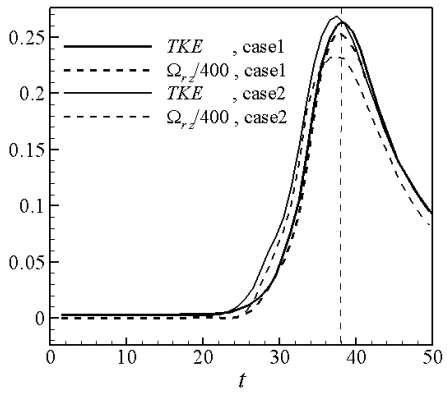

Fig. 5. Evolution of turbulent kinetic energy and enstrophy of loop-like and hair-pin vortices integrated over the whole domain.

ISSN: 2278 – 7798

[5] CONCLUSION

The interaction between a vortex ring and a flat plate has been studied by means of the large eddy simulation technique. The vortical flow phenomena and the underlying physical mechanisms were investigated and are summarized briefly as follows.

We investigate the effect of Reynolds number on the dynamics of vortex structures and the turbulent behaviour of flow. For high Reynolds number case, the total kinetic energy decreasing more quickly and larger amplitude of the enstrophy indicates that the flow dissipates more quickly. After the vortical structures break into small-scale vortices, the transition from laminar to turbulent state occurs. The turbulent behaviour can be analysed by the turbulent kinetic energy. Larger amplitude of the TKE indicates the stronger strength of turbulence for the high Reynolds number case. Moreover, it is found that the formation of the loop-like and hair-pin vortices plays an important role in the flow transition from laminar to turbulent state.

REFERENCES

[1] D. G. Akhmetov, B. A. Lugovtsov, and V. F. Tarasov, "Extinguishing gas and oil well fires by means of vortex rings," *Combust. Explos. Shock Waves*, vol. 16, pp. 490-494, 1980.

[2] G. L. Chahine, and P. F. Genoux, "Collapse of a cavitating vortex ring," *J. Fluid Eng.*, vol. 105, pp. 400-405, 1983.

[3] T. S. Lundgren, and N. N. Mansour, "Vortex ring bubbles," *J. Fluid Mech.*, vol. 224, pp. 177-196, 1991.

[4] M. Cheng, J. Lou, and L. S. Luo, "Numerical study of a vortex ring impacting a flat wall," *J. Fluid Mech.*, vol. 660, pp. 430-455, 2010.

[5] T. T. Lim, T. B. Nickels, and M. S. Chong, "A note on the cause of rebound in the head-on collision of a vortex ring with a wall," *Exp. Fluids.*, vol. 12, pp. 41-48, 1991.

[6] P. Orlandi, and R. Verzicco, "Vortex rings impinging on walls: axisymmetric and three dimensional simulations," *J. Fluid Mech.*, vol. 256, pp. 615-646, 1993.

[7] A. M. Naguib, and M. M. Koochesfahani, "On wall-pressure sources associated with the unsteady separation in a vortex-ring/wall interaction," *Phys. Fluids.*, vol. 16, pp. 2613-2622, 2004.

[8] C. C. Chu, C. T.Wang, and C. C. Chang, "A vortex ring impinging on a solid plane surface-Vortex structure and surface force," *Phys. Fluids A*, vol. 7, pp. 1391-1401, 1995.

[9] J. D. A. Walker, C. R. Smith, A. W. Cerra, and T. L. Doligalski, "The impact of a vortex ring on a wall," *J. Fluid Mech.*, vol. 181, pp. 99-140, 1987.

[10] P. G. Saffman, "The number of waves on unstable vortex rings," *J. Fluid Mech.*, vol. 84, pp. 625-639, 1978.

[11] K. Shariff, R. Verzicco, and P. Orlandi, "A numerical study of three-dimensional vortex ring instabilities: viscous corrections and early nonlinear stage," *J. Fluid Mech.*, vol. 279, pp. 351-375, 1994.

[12] M. Sreedhdar, and S. Ragab, "Large eddy simulation of longitudinal stationary vortices," *Phys. Fluids*, vol. 6, pp. 2501-2514, 1994.

[13] H. Ren, and X.Y. Lu, "Large eddy simulation of a vortex ring impinging on a three-dimensional circular cylinder," *Theor. Appl. Mech. Lett.*, vol. 3, 032007, 2013.

[14] H. Ren, and C. Y. Xu, "Three-dimensional numerical simulation of a vortex ring impacting a bump," *Theor. Appl. Mech. Lett.*, vol. 4, 032004, 2014.

Heng Ren received B. E. degree in Engineering Mechanics from Lanzhou University and Ph. D degree in Engineering Mechanics from University of Science and Technology of China. Presently working as an engineer in China Electronics Technology Group Corporation No.38 Research Institute. His research areas are electronic equipment thermal control and computational fluid dynamics.

ISSN: 2278 – 7798